Journal of
Ceramic Science
and Technology

J. Ceram. Sci. Tech., **03** [03] 151-158 (2012)
DOI: 10.4416/JCST2012-00015
available online at: http://www.ceramic-science.com

Processing of Nanostructured Zirconia Composite Ceramics with High Aging Resistance

M. Johannes, J. Schneider*

Fraunhofer Institute for Ceramic Technologies and Systems, Department of Oxide- and Polymer-Ceramic Components, Michael-Faraday-Strasse 1, 07629 Hermsdorf/Germany

received April 17, 2012; received in revised form June 11, 2012; accepted July 25, 2012

Abstract

Dense-sintered ceramic bodies of 3Y-TZP and ATZ (90 % ZrO_2-10 %Al_2O_3) composite ceramic were prepared from commercial powders by means of slip casting, sintering and hot isostatic pressing. The powders were processed in an optimized milling procedure. The properties of the milled particles were determined with diffusive light scattering, Rietveld refinement, BET and SEM. The enhanced sintering activity allows a decrease in the sintering temperature by more than 100 K. After hot isostatic pressing, samples with a grain size of ≈ 150 nm were obtained. These nanostructured ceramics are not affected by low-temperature degradation in hydrothermal atmosphere at 134 °C. No significant difference in fracture toughness between coarse-grained Y-TZP and nanostructured ceramics was observed. The bending strength of nanostructured Y-TZP is slightly reduced compared with coarse-grained Y-TZP. The prepared ATZ ceramic exhibits a bending strength of about 1700 MPa and a Weibull parameter of 14.

Keywords: Zirconia, Y-TZP, ATZ, ceramic composite, nanostructured ceramics, low-temperature degradation, stirred media mill

I. Introduction

During the last three decades, yttria-stabilized tetragonal zirconia polycrystal (Y-TZP) has been developed to a state-of-the-art ceramic material in many applications like mechanical engineering and chemical equipment. Since the late 1980s, Y-TZP has become more and more attractive as a bioceramic used for artificial hip and knee joints [1–5]. The St Gobain/Desmarquest scandal in 2001 with many revision operations owing to failed Y-TZP hip joint heads has damaged the good reputation of TZP as a bioceramic [6]. Recently, the upcoming dental market discovered Y-TZP as a promising material for dental implants, crowns and bridges [7].

The high fracture toughness and strength are associated with the stress-induced phase transformation of the metastable tetragonal phase into the stable monoclinic phase. The increase of the specific volume during the t-m phase transformation leads to compressive stress at the crack tip and counteracts crack propagation. This transformation toughening is described extensively in the literature [8–10]. The fracture toughness and bending strength of Y-TZP can reach 7 $MPam^{1/2}$ and 1200 MPa respectively.

Unfortunately, the phase transformation also occurs in the presence of water at elevated temperature. Such a hydrothermal atmosphere is, among other conditions, present in the body environment. This low-temperature degradation (LTD) leads to a decay of the surface properties like hardness and roughness. If there is sliding contact between Y-TZP parts, the LTD isaccompanied by a large amount of wear debris [11]. This may lead to aseptic loosening of the implant.

There are many models describing LTD [12–16]. In fact, we know a lot about the influencing factors and the sequence of LTD, but a fundamental description of the mechanism including all key parameters is still pending [17].

In general, LTD can be avoided by reducing the grain size below a critical value [18] and with a homogenous yttria distribution [19] assuming that the ceramic has at least 99 % of the theoretical density. These requirements can be achieved by using sufficient fine powders and low sintering temperatures [20]. Some groups worldwide have succeeded in the manufacturing of dense nanostructured 3Y-TZP ceramics from nanopowders [21–23]. The nano 3Y-TZP prepared by Binner *et al.* exhibits a grain size in the range of 90 to 130 nm and shows excellent aging resistance up to 250 °C and 336 h [24]. However, the use of nanopowders represents a high cost factor for the production of structural ceramics.

An alternative way to produce nanostructured ceramics involves the deagglomeration and comminution of submicron powder. Comminution in stirred media mills is a common powder processing technology in the ceramic industry, because the process parameters can be scaled up from laboratory mills to an industrial standard [25]. The high energy density in the grinding chamber enables the comminution of commercial submicron powder to small particle sizes with narrow particle size distributions [26,27]. Houivet *et al.* [28] described the fine grinding of oxide powders based on control of the viscosity and stability of the slurry with adaption of the pH value. The effectiveness of

* Corresponding author: jens.schneider@ikts.fraunhofer.de

stirred media mills with small grinding beads (< 100 μm) for the preparation of nanostructured zirconia ceramics is highlighted by Su°rez *et al.* [29,30]. All these grinding experiments were conducted with low-concentrated slurries (< 20 wt%), leading to comparatively poor green densities, so that high sintering temperatures were needed to achieve dense ceramic bodies.

The present work describes the influence of the grinding bead diameter on the particle size distribution in highly concentrated slurries of Y-TZP and Y-TZP-Al_2O_3 dispersions. Although Kern and Gadow [31,32] have shown that alternative stabilizers may enhance the mechanical properties and aging resistance, yttria-stabilized zirconia currently has the most commercial relevance. The use of commercial powders combined with a high throughput and short sintering duration promise great relevancy for industrial implementation of this technique. The structural changes of the powder during grinding are characterized and discussed. Furthermore, the sintering behavior and the microstructual features of the sintered 3Y-TZP and 3Y-TZP/Al_2O_3 ceramics are studied. Finally, the mechanical properties like hardness, strength and toughness as well as the hydrothermal aging resistance of the ceramics are tested.

II. Experimental

For the preparation of the sintered ceramic bodies a commercial zirconia powder (TZ3Y-SE, Tosoh Ltd., Japan) and high-purity alumina (TM-DAR, Taimei Chemicals, Japan) were used. A primary particle size of 70 nm for the TZ3Y-SE and 100 nm for the TM-DAR was specified by the manufacturers. Sample groups Z-1 and Z-2 are made of 100 % 3Y-TZP. The sample group ZA-10 consists of 90 wt% 3Y-TZP and 10 wt% Al_2O_3.

The powders were dispersed in water up to 65 wt% while the viscosity was adjusted to 20 mPas at a shear rate of 200 s^{-1} using 0.4 wt% ammonium polyacrylate (Zschimmer and Schwarz, Germany) relative to the solid content in the slurry. The slurry was milled for 120 min in a laboratory stirred media mill (Mini Cer, Netzsch FMT, Germany) with 3Y-TZP grinding beads. The grinding beads filled 80 % of the grinding chamber and the optimum tip speed of the stirrer was adjusted to 11 m/s. The grinding beads had a diameter of 500 μm for processing the Z-1 samples and 100 μm for the samples Z-2 and ZA-10. The pH value of the slurries varied between 9 and 10.

The particle size distribution in the slurries was measured with an Ultrafine Particle Analyzer (UPA, Microtrac, USA). After grinding, a small portion of the slurry was dried and the powder was investigated with SEM (Zeiss Ultra 55+; Carl Zeiss NTS Germany), BET (ASAP 2020, Micrometrics, Germany) and XRD (D8 Advance, Bruker, Germany). The quantitative phase analysis was performed with Rietveld refinement (AutoQuan, GE-Sensing Technology, Ahrensburg, Germany). The parameter setting used in the Rietveld analysis is described elsewhere [33]. BET measurements were conducted to determine the specific surface area and the equivalent particle diameter d_{BET} in accordance with Eq. 1. This value is comparable to the primary particle size of the powder.

The samples were shaped into plates with dimensions of 30 x 20 x 3 mm by means of slip casting and sintered at various temperatures in the range of 1200 °C and 1450 °C with heating and cooling rates of 3 K/minute. A dwell time of one hour was applied. Samples with at least 95 % theoretical density were subjected to hot isostatic pressing (HIP) for 2 h. The HIP-temperatures were equal to the particular sintering temperatures, applying a Ar-gas pressure of 14 MPa. The densities of the samples after HIP were determined with the Archimedes method. The phase composition and the microstructure of the dense ceramic bodies were investigated with XRD and SEM respectively. A detailed account of the results of the sintering and HIP experiments can be found in section III.

After HIP the samples were polished, reaching a roughness R_a of 8 nm for 3Y-TZP and 16 nm for the ATZ samples. The microstructure was investigated with SEM and the grain size was determined with the line intercept method as prescribed in EN 623 – 3. The samples were hydrothermally aged in an autoclave (Wolf-Sanoclav, Germany) at 134 °C and 2 bars for 192 h in water vapor. The phase composition of the aged samples was analyzed by means of XRD and Rietveld refinement and the microstructure was investigated with SEM. The 4-point bending strength and the Weibull statistics were determined on small size bars with dimensions of 2 x 2.5 x 25 mm in accordance with EN 843 – 1 and EN 843 – 5 respectively. The microhardness HV0.1 and HV10 with normal loads of 0.98 N and 98 N respectively was measured on the polished surfaces, applying the procedure described in EN 843 – 4. Furthermore, the fracture toughness was tested with both single-edge V-notch beams (SEVNB) according to CEN/TS 14425 – 5 and direct crack length measurement after a HV10 indentation (IF-method). The notch was cut in the sintered bars with a razor blade and diamond paste was used as the grinding medium. An average notch root width of 4 μm was achieved. The calculation of K_{IC} deduced from the IF-method was performed using the equations of Niihara [34] (Eq. 2) and Anstis [35] (Eq. 3), where E is the Young's modulus, ø a geometrical factor assuming ≈ 3, H the Vickers hardness, c the crack length, a the diagonal length of the indentation and P the indentation load. Young's modulus for Z-1 and Z-2 was assumed to be 210 GPa and for the ZA-10 sample 232 GPa was calculated by the rule of mixture.

$$d_{BET} = \frac{6}{s \cdot p} \tag{1}$$

$$K_{IC}(\text{Niihara}) = 0{,}048\ Ha^{0,5} \left(\frac{E\oslash}{H}\right)^{0,4} \left(\frac{c}{a}\right)^{-0,5} \tag{2}$$

$$K_{IC}(\text{Anstis}) = 0{,}014\ Ha^{0,5} \left(\frac{E}{H}\right)^{0,5} \left(\frac{P}{c^{1,5}}\right) \tag{3}$$

For evaluating the transformability of the tetragonal phase, the monoclinic phase fraction on the fractured surface of the SEVNB bars was determined with position-sensitive XRD

III. Results and Discussions

(1) Grinding and dispersing

Fig. 1 shows the d_{50} and the d_{95} value of the particle size distribution after grinding. Samples Z-2 and ZA-10 exhibit a smaller particle size and a narrower particle size distribution in the slurry.

The optimized grinding with small grinding beads leads to a decrease in the d_{50} value and a minimization of the d_{95} value. The d_{95} is an indicator of the number of broken aggregates and agglomerates. Fig. 2 visualizes that the most of agglomerates and aggregates broke up during grinding into primary particles with a diameter of approximately 100 nm. Some remaining aggregates up to 400 nm explain the d_{50} and d_{95} values measured with UPA.

The grinding process entails a rise in monoclinic phase, owing to stress-induced phase transformation of the tetragonal phase. The transformation energy consumes grinding energy and therefore leads to a reduction in grinding efficiency. The tetragonal crystallite size is decreased after grinding, which is apparent at the peak broadening in the X-ray scattering patterns in Fig. 3. The following characterization of structural changes as a result of grinding is only exemplified on the TZ3Y-SE powders of the charge Z-2 and is given in Table 1.

By means of the Rietveld refinement, the contents, the crystallite sizes and the microstrains of the tetragonal and monoclinic phase were calculated. The residuals of the phase contents up to 100 % are small amounts of the cubic phase. BET measurements indicate the increase of the specific surface area and the decrease of the equivalent particle diameter during grinding.

The decrease in the tetragonal crystallite size is not only an effect of particle comminution but rather an effect of stress-induced phase transformation. Thereby parts of the tetragonal crystallites transform into the monoclinic phase separating the tetragonal crystallites within a primary particle. Therefore, the primary particle size is not affected during short grinding periods. The crystallite size of the monoclinic phase is almost unchanged during grinding. The calculation of the microstrain of the tetragonal phase after grinding gave an error because all peak broadening parts including faults were put in the size parameter. Hence, the tetragonal crystallite size may be under-determined. The microstrain of the monoclinic phase was always higher than that of the tetragonal phase, because of lattice distortion during transformation.

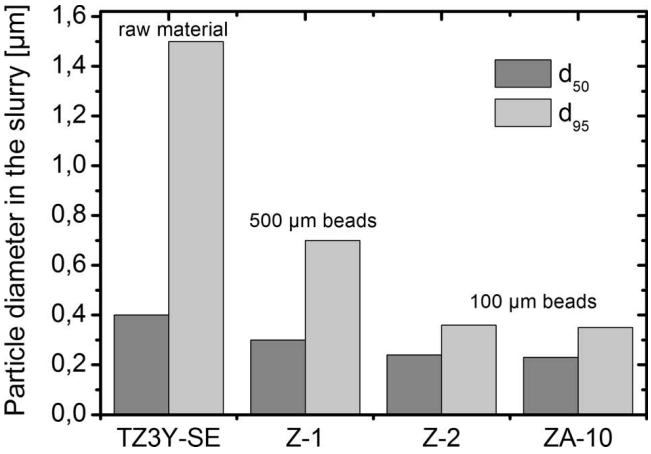

Fig. 1: Particle sizes d_{50} und d_{95} in the slurry measured after grinding.

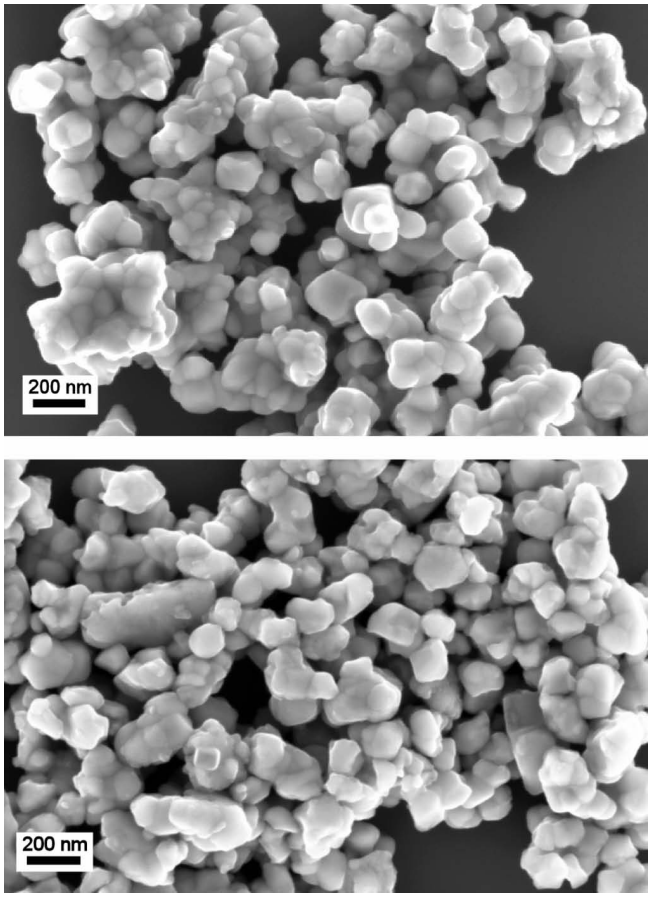

Fig. 2: SEM micrograph of the zirconia powder before and after grinding.

Table 1: Results from Rietveld refinement and BET measurements of the raw material and powder Z-2 after grinding.

Sample	Phase	Content [wt-%]	XRD crystallite size [nm]	Microstrain [%]	BET [m^2/g]	d_{BET} [nm]
TZ3Y-SE	tetragonal	72.7 ± 1.0	52 ± 4	0.2 ± 0.02	6.5 ± 0.04	150
	monoclinic	25.2 ± 0.8	30 ± 4	0.5 ± 0.07		
Z-2	tetragonal	55.7 ± 1.5	19 ± 1	-	10.3 ± 0.05	100
	monoclinic	43.0 ± 1.1	25 ± 3	0.6 ± 0.08		

The particle size obtained from BET measurements show a decrease in the primary particle size from 150 nm to 100 nm. These are the primary particles visible in Fig. 2.

(2) Molding and sintering

The slip-cast and dried green bodies achieved a density of 62 % of the theoretical density. The properties of the castings depend on many factors such as viscosity, dispersant content, solid content in the slurry, particle size distribution, properties of the mold material, temperature, etc. [36]. In principle, the sintering activity increases with decreasing particle size in the slurry and increasing homogeneity of the particle arrangement during cast formation [37].

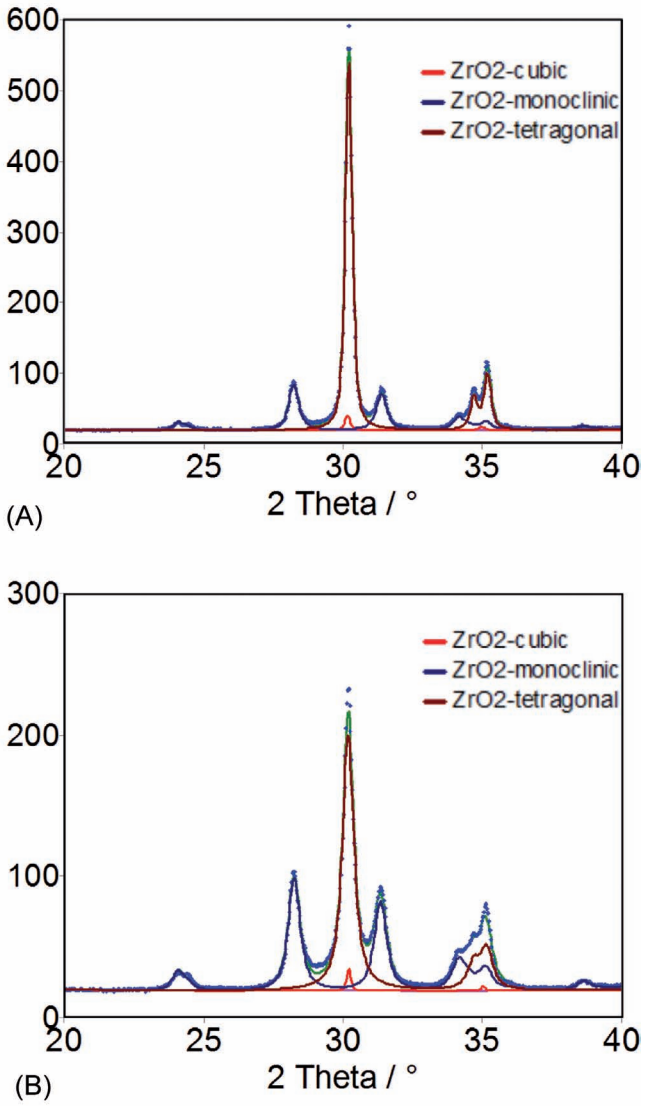

Fig. 3: XRD patterns and SEM micrographs of the zirconia powder TZ3Y-SE before grinding (A) and Z-2 after grinding (B); blue points: measured intensities; green line: whole pattern fitting curve.

In Fig. 4 the sintering density is plotted against the sintering temperature. The sintering activity of Z-2 and ZA-10 is much higher than that of Z-1 and therefore the desired densities are achieved at much lower temperatures. Finally, the samples were sintered and HIPed at 1450 °C (Z-1), 1250 °C (Z-2) and 1300 °C (ZA-10). The HIP process ensures that the remaining closed porosity after sintering will vanish without increasing the temperature. After HIP the relative densities of the sintered bodies reached at least 99.5 % of the theoretical density of 6.1 g/cm^3 for 3Y-TZP and 5.79 g/cm^3 for ATZ respectively. The theoretical densities were calculated by means of Rietveld refinement with provision for the chemical composition and the phase content of the as-fired samples.

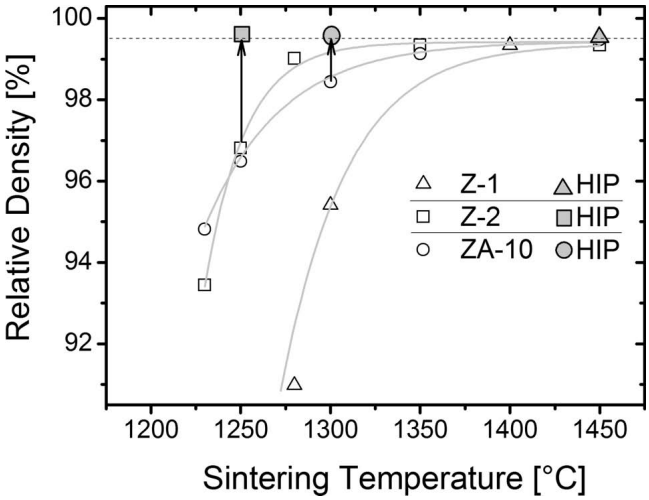

Fig. 4: Sintering curves of the slip-cast bodies, the arrows indicate the density after the HIP step.

The SEM micrographs in Fig. 5 demonstrate the effect of the low sintering temperature in respect of the grain size. The grain sizes determined from the SEM micrographs are 340 ± 30 nm for Z-1, 150 ± 30 nm for Z-2 and 143 ± 40 nm for ZA-10. Some large grains are visible in the fine-grained microstructure as of result of residual agglomerates. There is a relation between the grain sizes of the dense-sintered ceramics and the d_{95} particle sizes in the slurry shown in Fig. 1. Therefore, the particle size distribution in the slurry is assumed to be a key parameter in avoiding undesired grain growth.

The phase composition and crystallite sizes of the dense-sintered bodies are presented in Table 2. No evidence of monoclinic phase is shown. The cubic phase content increases with the increasing sintering and HIP temperature, which can also be derived from the equilibrium composition in the phase diagram [38]. Alumina has a restraining effect on the formation of cubic phase. The crystallite size correlates with the measured grain size. The cubic crystallites are very small and it is not supposed that these form single cubic grains. Instead, cubic phase is considered to be small areas located on the grain boundaries where yttria tends to segregate. Further, it can be stated that the addition of 10 wt% alumina has a beneficial effect on the grain size and the crystallite size of the tetragonal phase in $^{Y\text{-}TZP}$ and impedes the formation of cubic phase.

(3) Mechanical properties

An additional stabilization of the tetragonal phase owing to small grain size may also affect the strength and toughness of the nanostructured ceramics. The mechanical properties of the 3Y-TZP and ATZ specimens are given in Table 3.

Table 2: Phase composition and phase crystallite sizes d_{XRD} of the dense ceramic bodies, the error is defined as the 3-fold standard deviation given by the Rietveld program.

	Z-1		Z-2		ZA-10	
Phase	wt%	d_{xrd} [nm]	wt%	d_{xrd} [nm]	wt%	d_{xrd} [nm]
ZrO_2 tetragonal	75.9 ± 1.6	280 ±45	83.2 ± 1,8	154 ± 18	77.6 ± 1.7	108 ± 10
ZrO_2 cubic	23.5 ± 1.6	22 ± 2	15.7 ± 1.9	11 ± 1	11.7 ± 1.7	12 ± 2
ZrO_2 monoclinic	0.0		0.3 ± 0.2		0.3 ± 0,2	
$Zr_3Y_4O_{12}$	0.6 ± 0.3		0.9 ± 0.3		1.0 ±0.3	
Y_2O_3	0.0		0.0		0.0	
Al_2O_3					9.4 ± 0.5	80 ± 10

Table 3: Mechanical properties of 3Y-TZP and ATZ ceramics after HIP.

		Z-1	Z-2	ZA-10
Bending Strength	MPa	1300 ± 100	1100 ± 170	1700 ± 100
Weibull Modulus m	-	13	9	14
Microhardness HV0.1	GPa	14.3 ± 0.7	20.4 ± 0.9	18.9 ± 2.0
Macrohardness HV10	GPa	13.28 ± 0.05	14.00 ± 0.03	15.28 ± 0.07
Fracture Toughness (SEVNB)	MPa $m^{1/2}$	8.8 ± 0.3	10.3 ± 0.6	9.1 ± 0.7
Fracture Toughness (Anstis)	MPa $m^{1/2}$	3.4	3.6	3.6
Fracture Toughness (Niihara)	MPa $m^{1/2}$	4.6	4.8	4.7
Transformability (m-ZrO_2 on the fracture surface)	wt-%	10.5	2.5	2.9

As expected, the strength of Z-2 is slightly reduced in comparison to sample Z-1, possibly because of an excess stabilization of the tetragonal phase. This agrees exactly with the results of Binner *et al.* [24], who overcome this problem by reducing the stabilizer content of the Y-TZP nanoceramics. Consequently, a correlation between aging resistance and strength based on grain size and stabilizer content is assumed and this will be the subject of further research.

In the present work, a small addition of alumina (ZA-10) leads to strength of 1700 MPa by a Weibull parameter of 14. A possible explanation of this behavior is that the thermal mismatch of zirconia and alumina creates local tensile stresses in the zirconia matrix next to the alumina grains during cooling. This may enhance the driving force for the martensitic phase transformation in the zirconia matrix.

A significant increase of the microhardness of about 40 % could be observed in the nanostructured sample Z-2 in comparison to the coarser-grained sample Z-1. HV10 measurements yield only slightly changed hardness values. The hardness of the Y-TZP ceramics shows a considerable influence of the grain size, which is known principally from the literature [39]. Furthermore, microhardness measurements are more sensitive to changes in the grain size than macrohardness measurements [40]. The large increase in microhardness raises expectations of improved wear resistance of the fine-grained compared to conventional 3Y-TZP.

The fracture toughness values of the ceramics determined by means of different methods are compared in Table 3. The absolute values differ widely between the test methods; however, the relative comparison of the samples gives consistent results. No decrease in fracture toughness is observed for the nanostructured 3Y-TZP. The K_{IC} value of 3.6 $MPam^{0.5}$ for sample Z-2 is comparable to the nanostructured 3Y-TZP published by Paul *et al.* [41] (3.6 $MPam^{0.5}$). The difference between the two IF methods has a numerical reason. Anstis' method considers median cracks whereas Niihara takes Palmqvist cracks into account. Although, the IF method has been heavily criticized recently [42], the SEVNB method presents considerable difficulties too [43]. The notch root diameter exceeds the grain size by more than one magnitude [44]. Furthermore, phase transformations on the notch root induced during grinding may affect the exact measurement of K_{IC}. To avoid such uncertainties, the samples could be notched in the green state or an annealing step could be added after notching [45].

Based on the small grain size, a higher stability of the tetragonal phase and hence a lower toughness because of constrained transformability may be expected [46]. The transformability is characterized by the amount of monoclinic phase on the fracture surface after SEVNB testing. The monoclinic phase content drops markedly down to 2.5 % when the grain size is reduced. It cannot be assumed

that such tiny transformation zones provide a noticeable contribution to fracture toughness. These unexpected results and the fact that the high fracture toughness of the fine-grained ceramic is not transformation-controlled call for further studies of the toughening mechanism of these materials.

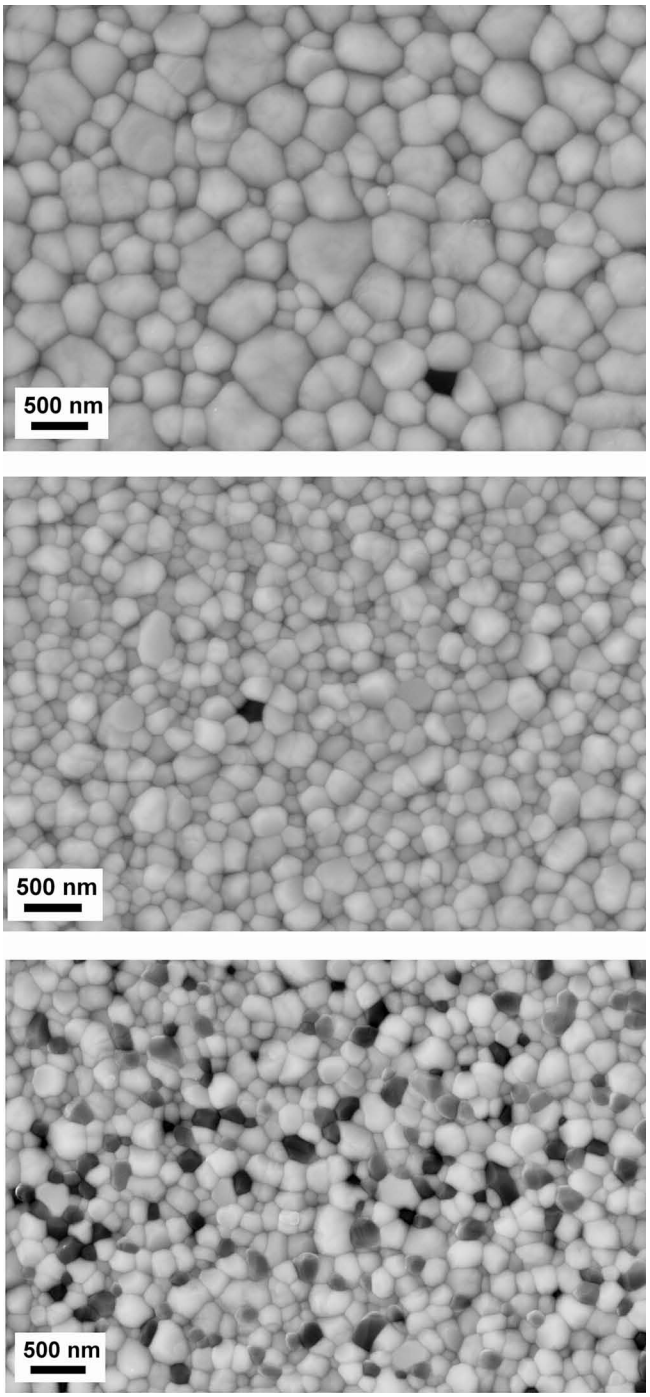

Fig. 5: FESEM micrographs of the sintered specimens; bright grains: zirconia; dark grains: alumina.

(4) Hydrothermal aging behavior

The low-temperature aging behavior was investigated in accelerated aging tests in an autoclave at a temperature of 134 °C and 2 bar water vapor pressure. In Fig. 6, the monoclinic phase content is shown as a function of the aging time.

Sample Z-1 exhibits a rapid increase in the monoclinic phase content in just a few hours in the aging environment. Compared to other coarse-grained 3Y-TZP, the aging resistance of sample Z-1 is not bad and fulfills the requirements of ISO 13356 (zirconia implants for surgery). The transformation rate lies somewhere between commercial 3Y-TZP and ATZ (80 % ZrO_2/20 % Al_2O_3) [11]. The samples Z-2 and ZA-10 are not subjected to low-temperature degradation even after 192 h in the hydrothermal environment. The aging resistance of Z-2 and ZA-10 is mainly based on their small grain size. Consequently, there is an increase in grain boundary energy and a decrease in local stress states at the grain edges and corners. Moreover, the low sintering temperature leads to a homogeneous stabilizer distribution. These thermodynamically contributions stabilize the tetragonal phase and prevent the martensitic phase transformation at least at 134 °C. Although other authors have tested their TZP materials at temperatures above 200 °C, it could be assumed that Z-2 and ZA-10 are hydrothermally stable even at temperatures above 134 °C when they survive 192 h without any evidence of aging [24].

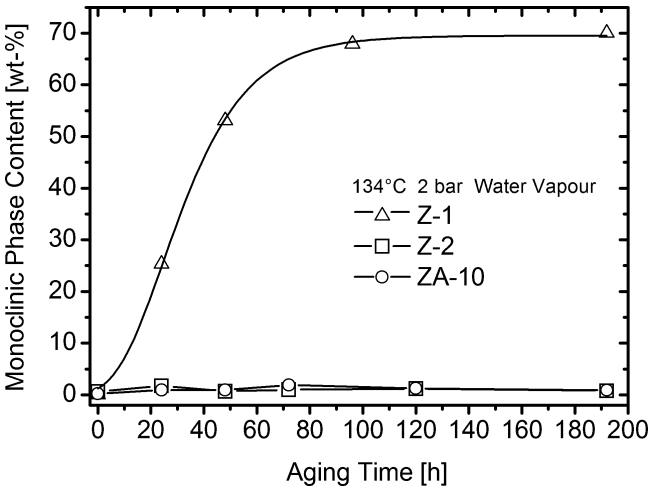

Fig. 6: Monoclinic phase content during aging in water vapor at 134 °C and 2 bar.

In Fig. 7, SEM micrographs of the polished cross-sections of the aged samples are shown. As expected, sample Z-1 with an average grain size of 340 nm exhibits a porous transformed layer with a thickness of about 10 μm. Samples Z-2 and ZA-10 show no damage or changes in the microstructure during hydrothermal aging.

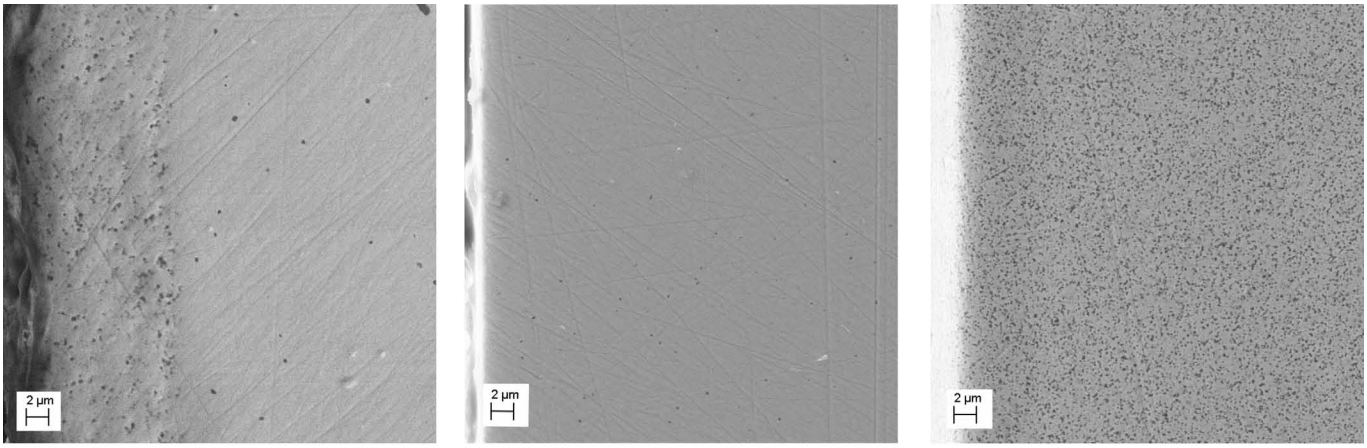

Fig. 7: FESEM micrographs of polished cross-sections of the hydrothermally treated samples.

IV. Summary and Conclusion

The grain size of advanced zirconia and composite ceramics depends strongly on the grinding and dispersing parameters of the powders. Thus, it is possible to produce nanostructured zirconia ceramics from commercial submicron powders by controlling the process parameters and the material properties during grinding. BET, XRD with Rietveld refinement, SEM and particle size measurements are suitable tools to control the process and ensure production quality. All grinding parameters obtained from laboratory mills can be scaled up to industrial standards. The use of small grinding beads with diameters equal to or smaller than 100 µm makes it possible to achieve a narrow grain size distribution and enhanced sintering activity of the powder. The samples could be molded only by slip casting. Behavior during cold isostatic pressing of spray-dried nanosized powders will be investigated in further studies.

The produced ceramics are resistant to aging even after 192 h at 134 °C in water vapor. Nanostructured Y-TZP exhibits a slightly lower bending strength than Y-TZP with submicron grain size owing to excess stabilization of the tetragonal phase. However, the high fracture toughness remains almost unaffected by the grain size, although the transformability of the nanostructured Y-TZP ceramic is drastically reduced. Other toughening mechanisms like grain boundary sliding have to be considered in further investigations. In spite of excess stabilization of the tetragonal phase, ATZ ceramic with 10 wt% Al_2O_3 reaches a bending strength of about 1700 MPa. The nanostructured Y-TZP exhibits an increase in microhardness of about 40 % compared with coarser grained Y-TZP ceramic.

Nevertheless, the presented manufacturing method may be a contribution to the generation of a new grade of zirconia matrix ceramics. The very short production time and the high throughput open the way to industrial application.

Acknowledgement

The authors are grateful to the German Federal Ministry of Economics and Technology (BMWi) for its financial support of the "Struktodent" Project, reference number MF090111.

References

1 Willmann, G., Früh, H.J., Pfaff, H.G.: Wear characteristics of sliding pairs of zirconia (Y-TZP) for hip endoprostheses, *Biomaterials*, **17**, 2157 – 2162, (1996).

2 Piconi, C., Burger, W., Richter, H.G., Cittadini, A., Maccauro, G., Covacci, V., Bruzzese, N., Ricci, G.A., Marmo, E.: Y-TZP ceramics for artificial joint replacements, *Biomaterials*, **19**, 1489 – 1494, (1998).

3 Piconi, C., Maccauro, G.: Zirconia as a ceramic biomaterial, *Biomaterials*, **20**, 1 – 25, (1999).

4 Cales, B.: Zirconia as a sliding Material: Histologic, laboratory, and clinical data, *Clin. Orthop. Rel. R.,* **379**, 94 – 112 (2000).

5 Sida, D., Blaise, L., Sida, V., Vavrik, P.: Zirconia ceramic femoral components, *Key Eng. Mat.*, **218 – 220**, 581 – 584, (2001).

6 Chevalier, J., Gremillard, L., Virkar, A.V., Clarke, D.R.: The tetragonal-monoclinic transformation in Zirconia: Lessons learned and future trends, *J. Am. Ceram. Soc.*, **92**, 1901 – 1920, (2009).

7 Kosmac, T., Dakskobler, A.: Tetragonal zirconia (Y-TZP) ceramics for dental applications: Criteria for materials selection, in: *Global Roadmap for Ceramics, International Congress on Ceramics, **ICC** 2*, 1 – 10, (2008).

8 Claussen, N., Ruehle, M., Heuer Arthur, H. (eds.): Phase transformations in ZrO_2- containing Ceramics: II the martensitic reaction in t-ZrO_2, *Science and Technology of Zirconia II,* **12**, American Ceramic Soc Inc, Stuttgart, (1984).

9 Lange, F.F.: Transformation toughening – part 1 size effects associated with the thermodynamics of constrained transformations, *J. Mater. Sci.*, **17**, 225 – 234, (1982).

10 Lange, F.F.: Transformation toughening – part 3 experimental observations in the ZrO_2-Y_2O_3 system, *J. Mater. Sci.*, **17**, 240 – 246, (1982).

11 Chevalier, J., Gremillard, L.: Ceramics for medical applications: A picture for the next 20 years, *J. Eur. Ceram. Soc.,* **29**, 1245 – 1255, (2009).

12 Sato, T., Shimada, M.: Transformation of yttria-doped tetragonal ZrO_2 polycrystals by annealing in water, *J. Am. Ceram. Soc.*, **68**, 356 – 356, (1985).

13 Lange, F.F., Dunlop, G.L., Davis, B.I.: Degradation during aging of transformation toughened ZrO_2-Y_2O_3 materials at 250 °C, *J. Am. Ceram. Soc.*, **69**, 237 – 240, (1986).

[14] Yoshimura, M., Noma, T., Kawabata, K., Somiya, S.: Role of H_2O on the degradation process of Y-TZP, *J. Mater. Sci. Let.*, **6**, 465 – 467, (1987).

[15] Schubert, H., Frey, F.: Stability of Y-TZP during hydrothermal Treatment: Neutron experiments and stability considerations, *J. Eur. Ceram. Soc.*, **25**, 1597 – 1602, (2005).

[16] Guo, X.: Property degradation of tetragonal zirconia induced by low-temperature defect reaction with water molecules, *Chem. Mater.,* **16**, 3988 – 3994, (2004).

[17] Chevalier, J.: What future for zirconia as a biomaterial? *Biomaterials,* **27**, 535 – 543, (2006).

[18] Becher, P.F., Swain, M.V.: Grain-Size-dependent transformation behavior in polycrystalline tetragonal zirconia, *J. Am. Ceram. Soc.*, **75**, 493 – 502, (1992).

[19] Basu, B., Vleugels, J., van der Biest, O.: Transformation behaviour of tetragonal Zirconia: Role of dopant content and distribution, *Mat. Sci. Eng. A Struct.*, **366**, 338 – 347, (2004).

[20] Matsui, K., Horikoshi, H., Ohmichi, N., Ohgai, M., Yoshida, H., Ikuhara, Y.: Cubic-formation and grain-growth mechanisms in tetragonal zirconia polycrystal, *J. Am. Ceram. Soc.*, **86**, 1401 – 1408, (2003).

[21] Vasylkiv, O., Sakka, Y., Skorokhod, V.V.: Low-temperature processing and mechanical properties of zirconia and zirconia-alumina nanoceramics, *J. Am. Ceram. Soc.*, **86**, 299 – 304, (2003).

[22] Trunec, M., Maca, K.: Compaction and pressureless sintering of zirconia nanoparticles, *J. Am. Ceram. Soc.*, **90**, 2735 – 2740, (2007).

[23] Binner, J., Annapoorani, K., Paul, A., Santacruz, I., Vaidhyanathan, B.: Dense nanostructured zirconia by two stage conventional/hybrid microwave sintering, *J. Eur. Ceram. Soc.,* **28**, 973 – 977, (2008).

[24] Binner, J., Vaidhyanathan, B., Paul, A., Annaporani, K., Raghupathy, B.: Compositional effects in nanostructured yttria partially stabilized zirconia, *Int. J. Appl. Ceram. Tec.*, **8**, 766 – 782, (2011).

[25] Zheng, J.: Stirred media mills: Dynamics, performance, and physio-chemical aspects. ProQuest Dissertations and Theses, ISBN: 9780591393316, Columbia University, (1997).

[26] Mende, S., Stenger, F., Peukert, W., Schwedes, J.: Production of sub-micron particles by wet comminution in stirred media mills, *J. Mater. Sci.*, **39**, 5223 – 5226, (2004).

[27] Stenger, F., Mende, S., Schwedes, J., Peukert, W.: The influence of suspension properties on the grinding behavior of alumina particles in the submicron size range in stirred media mills, *Powder Technol.*, **156**, 103 – 110, (2005).

[28] Houivet, D., Quercioli, R., Itaalit, B., Kassas, A., Kamlo, A.N., Bernard, J., Haussonne, J.-M.: Ultrafine grinding of oxide powders with a controlled viscosity of slurries, *Adv. Eng. Mater*., **13**, 609 – 615, (2011).

[29] Suárez, G., Sakka, Y., Suzuki, T.S., Uchikoshi, T., Zhu, X., Aglietti, E.F.: Effect of starting powders on the sintering of nanostructured ZrO_2 ceramics by colloidal processing, *Sci. Technol. Adv. Mat.*, **10**, 1 – 8, (2009).

[30] Suárez, G., Borodianska, H., Sakka, Y., Aglietti, E.F., Vasylkiv, O.: Zirconia nanoceramic via redispersion of highly agglomerated nanopowder and spark plasma sintering, *J. Nanosci. Nanotechno.*, **10**, 6634 – 6640, (2010).

[31] Kern, F.: 2.75Yb-TZP ceramics with high strength and aging resistance, *J. Ceram. Sci. Tech.*, **2**, 147 – 154, (2011).

[32] Gadow, R., Kern, F.: Novel zirconia – alumina nanocomposites combining high strength and toughness, *Adv. Eng. Mater.*, **12**, 1220 – 1223, (2010).

[33] Schneider, J., Begand, S., Kriegel, R., Kaps, C., Glien, W., Oberbach, T.: Low-temperature aging behavior of alumina-toughened zirconia, *J. Am. Ceram. Soc.*, **91**, 3613 – 3618, (2008).

[34] Niihara, K.: A fracture mechanics analysis of indentation-induced palmqvist crack in ceramics, *J. Mater. Sci. Let.*, **2**, 221 – 223, (1983).

[35] Anstis, G.R., Chantikul, P., Lawn, B.R., Marshall, D.B.: A critical evaluation of indentation techniques for measuring fracture Toughness: I, direct crack measurements, *J. Am. Ceram. Soc.*, **64**, 533 – 538, (1981).

[36] Tiller, F.M., Hsyung, N.B.: Theory of filtration of ceramics: II, Slip casting on radial surfaces. *J. Am. Ceram. Soc.*, **74**, 210 – 218, (1991).

[37] Krell, A., Hutzler, T., Klimke, J.: Transmission physics and consequences for materials selection, manufacturing, and applications, *J. Eur. Ceram. Soc.*, **29**, 207 – 221, (2009).

[38] Yashima, M., Kakihana, M., Yoshimura, M.: Metastable-stable phase diagrams in the zirconia-containing systems utilized in solid-oxide fuel cell application, *Solid State Ionics,* **86 – 88**, 1131 – 1149, (1996).

[39] Krell, A.: Load dependence of hardness in sintered submicrometer Al_2O_3 and ZrO_2, *J. Am. Ceram. Soc.*, **78**, 1417 – 1419, (1995).

[40] Kern, F.: Sintering conditions, microstructure and properties of alumina 10 vol% zirconia nanocomposites, *J. Ceram. Sci. Tech.*, **3**, 1 – 8, (2012).

[41] Paul, A., Vaidhyanathan, B., Binner, J.G.P.: Hydrothermal aging behavior of nanocrystalline Y-TZP ceramics, *J. Am. Ceram. Soc.,* **94,** (7), 2146 2152, (2011).

[42] Quinn, G.D., Bradt, R.C.: On the vickers indentation fracture toughness test, *J. Am. Ceram. Soc.*, **90**, 673 – 680, (2007).

[43] K°bler, J.: Fracture toughness of ceramics using the SEVNB method. Round Robin VAMAS Report No. 37. Empa-D°bendorf, Switzerland, (1999).

[44] Fischer, H., Waindich, A., Telle, R.: Influence of preparation of ceramic SEVNB specimens on fracture toughness testing results, *Dent. Mater.*, **24**, 618 – 622, (2008).

[45] Krell, A.: Features of notch preparation for fracture toughness measurements in partially stabilized zirconia. *J. Am. Ceram. Soc.*, **77**, 600 – 602, (1994).

[46] Bravo-Leon, A., Morikawa, Y., Kawahara, M., Mayo, M.J.: Fracture toughness of nanocrystalline tetragonal zirconia with low yttria content, *Acta Mater.*, **50**, 4555 – 4562, (2002).